Hybrid density functional calculations of the surface electronic structure of GdN

Lukas Eugen Marsoner Steinkasserer,[1,2,*] Beate Paulus,[1] and Nicola Gaston[2]

[1]*Institut für Chemie und Biochemie, Freie Universität Berlin, Takustraße 3, 14195 Berlin, Germany*

[2]*MacDiarmid Institute for Advanced Materials and Nanotechnology, School of Chemical and Physical Sciences, Victoria University of Wellington, P.O. Box 600, 6140 Wellington, New Zealand*

(Received 16 January 2015; revised manuscript received 22 April 2015; published 29 June 2015)

Rare-earth nitrides are a promising class of materials for application in spintronics, with GdN a particularly well-studied example. Here we perform band-structure calculations employing a hybrid density functional, which enables the band gap to be more accurately predicted through the inclusion of short-range exact exchange. The sensitivity of the band gap to the exchange term is demonstrated. The surface electronic structure is simulated through the use of slab models of the GdN(111) surface, which provide a consistent description of metallic surface states in the majority-spin channel.

DOI: 10.1103/PhysRevB.91.235148 PACS number(s): 71.15.Ap, 71.20.Eh, 73.20.Hb

I. INTRODUCTION

The field of spintronics has grown rapidly since the discovery of the giant magnetoresistive effect in 1988 [1–3], and the inclusion of spin information into classical electronics promises great potential in terms of expanding and surpassing present-day computing capabilities [4]. However, the availability of magnetic semiconductors, which are capable of exploiting spin information within the context of transistor technology, is crucial for the practical realization of this potential.

Around the middle of the 20th century, a promising set of candidates to fulfill these expectations was found in the form of rare-earth nitrides (RENs) [5]. Their strong magnetic moments combined with a wide variety of band-gap values and other physical properties make them an ideal candidate for spintronic transistor applications. Although RENs were plagued initially by grave practical difficulties, recent advances in their experimental preparation and study have brought them back as a focus of research.

Much progress has been made in the field of RENs, but many questions still remain. In particular, the electronic structure of RENs has been a subject of lively discussions, with historical data on band gaps and other properties often varying widely [5]. Only recently has a consensus started to emerge regarding the properties of some of the RENs. Chief among these has been GdN, whose strong magnetic moment, together with its vanishing indirect and small direct band gap, render it a very promising research target. GdN, like all RENs, adopts a fcc NaCl structure [space group $Fm\bar{3}m$ (225)]. While experimental studies have been hindered by difficulties in the preparation of thin films, theoretical investigations have suffered from problems associated with the accurate description of strongly correlated f electrons within the context of density functional theory (DFT).

The standard way to address these problems is via the well-known DFT+U approach [6]. This method yields results that are in good agreement with experiment, but the theoretical insight obtained from it is limited by the need to carefully calibrate the U parameter in order to reproduce experimental results (usually experimental band-gap data). One of the alternative ways to overcome these problems while staying within the DFT framework is via the use of so-called hybrid functionals in which exchange calculated via Kohn-Sham orbitals (exact exchange) is included in the equations defining the DFT exchange functional.

Many studies have been published on GdN using the DFT+U method [7–21], but only a few attempts have been made to address the problems associated with obtaining an accurate description of strongly correlated f electrons in a more *ab initio* way [22–28], and no thorough investigation into the effect of the exact exchange fraction in hybrid functionals has yet been attempted. Even more striking, however, is the apparent complete lack of theoretical work on the behavior of GdN surfaces. This is all the more important since surface effects should play an important role in practical applications of GdN-based devices such as transistors.

To address these problems and hopefully pave the way for future research, we present herein a systematic investigation of the effect of short-range exact exchange on the band-structure characteristics of GdN. We further demonstrate the ability of state-of-the-art plane-wave hybrid DFT within the projector augmented wave framework to study the GdN (111) surface and to gain valuable insight from surface band-structure calculations.

II. COMPUTATIONAL DETAILS

All of the calculations in this work were performed using the Vienna ab-initio simulation package (VASP) [29–32] within the projector augmented wave method (PAW) [33,34] employing the HSE06 screened hybrid functional [35–39]. Bulk calculations were performed employing a $6 \times 6 \times 6$ k-grid for structure relaxations, while a $10 \times 10 \times 10$ k-grid was used to compute the band structure. In all cases, an energy cutoff of $\approx$590 eV was used in order to avoid Pulay-stress-related errors during structural relaxation, and to achieve high levels of accuracy across all calculations. Brillouin zone integration of band-structure-dependent functions (e.g., the densities of states and charge densities) was performed using Gaussian smearing with a smearing width equal to 0.05 eV. Both bulk as well as surface relaxations were considered to be

*marsoner@zedat.fu-berlin.de

converged if Hellmann-Feynman forces on nonfixed atoms (in the case of surface calculations) or stress acting on the unit cell (in the case of bulk relaxations) were lower than 0.01 eV/Å.

Surface calculations on the GdN(111) surface were performed using six Gd(N) layers and five N(Gd) layers for the Gd(N)-terminated surfaces (see Fig. 3). A vacuum separation of 20 Å was used to avoid unphysical interactions between periodic images of the slab. Structural relaxations were performed for the asymmetric slabs by keeping the bottom two atomic layers (one Gd, one N) fixed while all other atoms were allowed to relax along the surface-normal direction. In the case of symmetric slabs, the central three atomic layers (one Gd, two N) were fixed. Surface calculations employed a $6 \times 6 \times 1$ k-grid for structure relaxations, while a $10 \times 10 \times 1$ k-grid was used to compute the band structure. Brillouin zone integration was done using Methfessel-Paxton smearing with a smearing width equal to 0.4 eV in the Gd-terminated and 0.18 eV in the N-terminated case. The smearing factors were chosen so as to result in entropy values $\approx$1.0 meV/atom for the k-grid used during structure relaxation.

III. RESULTS

As a first step in setting up all further calculations and also as a verification of the accuracy of our chosen method, we performed a full relaxation of the GdN bulk unit cell and compared the results to experimental values. For this purpose, the standard HSE06 functional is used, which includes 25% of short-range exact exchange. Full relaxation yielded a theoretical lattice constant of 4.980 Å, which is in excellent agreement with the experimentally reported value of 4.974 Å [40].

The relaxed structure was then used for band-structure calculations, the results of which are shown in Fig. 1. The band structure is in line with previously reported theoretical results, showing a negligible indirect ($\Gamma \rightarrow X$) band gap as well as a direct ($X \rightarrow X$) gap of 0.47 and 1.86 eV for the two spin channels, respectively. The numerical values for the band gaps agree very well with the results obtained by Schlipf *et al.* within the full potential linearized augmented plane wave (FLAPW) method using the HSE06 functional; they obtained band gaps of 0.49 and 1.85 eV for the two spin channels, respectively [22,23]. This compares to previous experimental values of 0.90 and 1.72 eV [14], and most recently to values of 1.12 and 1.58 eV [41] in near-infrared absorbance spectroscopy experiments, which also produce a larger indirect band gap of 0.81 eV.

As Gd electrons are known to exhibit strong spin-orbit coupling, which, through its influence on the Gd-d bands, influences the electronic band structure in the valence region of GdN [7,17,18], on the right-hand side of Fig. 1 we have included spin-orbit coupling into the calculation of the band structure. While the effect of including spin-orbit coupling on the Gd-f electrons is as expected very strong, the valence region changes only slightly, with the direct ($X \rightarrow X$) gap decreasing from 0.47 eV for the spin-polarized calculation to 0.32 eV in the spin-orbit coupled case. This decrease of 0.14 eV agrees reasonably well with what was observed by Larson and Lambrecht [7] in their LDA+U calculations within the FLAPW method. They calculated a direct majority-spin gap at X equal to 0.57 eV, which decreased to 0.50 eV when spin-orbit coupling was included.

Due to the relatively small magnitude of the effect of spin-orbit coupling on the valence-region electronic band structure and the high computational cost associated with it, we have opted to perform all surface calculations without the inclusion of spin-orbit coupling. We retain that, while the quantitative values of the band energies will be affected by the inclusion of spin-orbit coupling, all the qualitative conclusions are still valid and allow us to gain insight into the characteristics of the GdN surface electronic structure.

An interesting feature, apparent when analyzing the local nature of the bands shown in Fig. 1, is the contribution of Gd and N atoms, respectively, to the total band structure of the compound. The nature of the band gap at the X point is that of a N $\rightarrow$ Gd charge transfer. This is consistent with previous reports [41], and it has interesting consequences for the band structure of other Gd pnictides in which the maximum in band energy, which touches the Fermi energy at the Γ point in the GdN case, is strongly shifted above E_F to form a hole pocket, while strong hybridization is present at the X point [42].

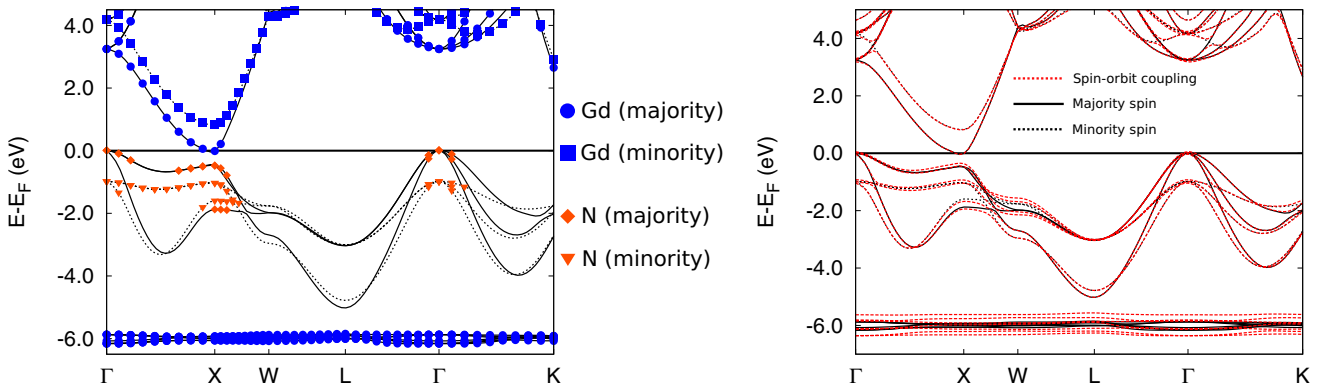

FIG. 1. (Color online) Bulk band structure of GdN at the HSE06-optimized lattice constant. The left-hand figure shows the results of spin-polarized hybrid-DFT calculation, while on the right-hand site we have included spin-orbit coupling. For the spin-polarized case, local projections on the Gd and N atoms with a local contribution of at least 75% are also shown. In both cases, majority- and minority-spin bands are indicated as full and dotted black lines, respectively, while spin-orbit coupled bands are indicated in red.

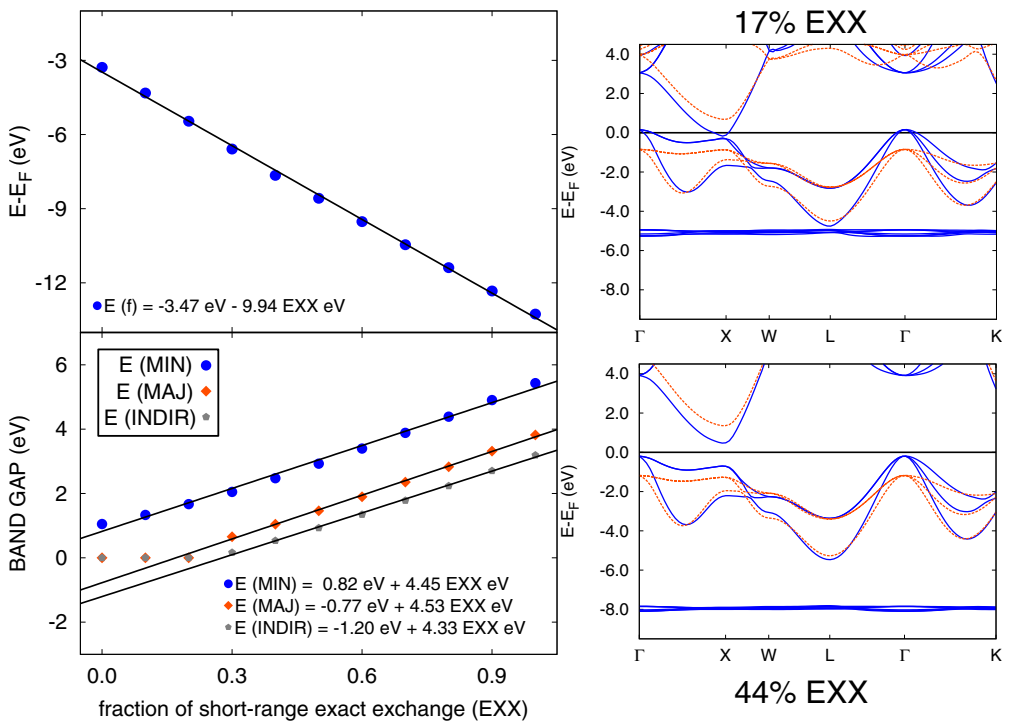

FIG. 2. (Color online) Band gap (bottom) and averaged position of the occupied f bands with respect to the Fermi energy (top) for calculations using a screened hybrid functional based on HSE06, including varying fractions of short-range exact exchange. The band-gap values are calculated at the X point for the direct majority [E(MAJ)] and minority [E(MIN)] gap while E(INDIR) indicates the value for the indirect ($\Gamma \rightarrow X$) gap. The average f-electron energy is taken at the Γ point. Note that a fit for the minority-spin gap, ignoring the value obtained for zero exact exchange, gives $E = 0.72 + 4.60\ EXX$. On the right-hand side, two band structures, calculated employing short-range exact exchange fractions of 17% (top) and 44% (bottom), are also shown. These represent the results of the linear fits for a zero direct (X-point) band gap in the majority-spin channel (17%) as well as the experimentally observed XPS peak corresponding to the Gd^{3+} $4f^6$ final state multiplet at $E - E_F = -7.8$ eV [43] (44%). Here, majority- and minority-spin bands are shown as full-blue and dotted-red lines, respectively.

A. The effect of short-range exact exchange

It is known [5] that the results of commonly employed DFT+U calculations on GdN depend heavily upon the exact value of the fitting parameters. Within the hybrid DFT formalism, the amount of short-range exact exchange included in the functional plays a similar role to that of U and J in DFT+U, although, as it is an evenly and globally applied "fitting parameter", it may be seen to do so on a firmer footing. The effect of employing different types of DFT functionals/methods, such as HF, the HSE/PBE0 functionals including 25% of exact exchange, and the B3LYP functional (20%), has already been discussed in the literature [22,23,25]. These results do not allow us to draw clear conclusions as to the exact effect that the fraction of exact exchange (in the HF, PBE0, and B3LYP case) or the screened, i.e., short-range exact exchange (in the HSE06 case) has on the system's band structure. This is due to the fact that all of the above methods differ in the details of the exchange-correlation treatment they employ, and so effects stemming from those cannot be separated from differences originating from the fraction of exact/screened exchange. The choice of HSE06 over other DFT functionals is further motivated by the physically justified screening of exchange, as well as the pragmatic advantage that this allows for numerical efficiencies. To exclude possible effects due to the different DFT exchange-correlation functionals, such as those used within the B3LYP versus the HSE06 hybrid functionals, we have performed all of the calculations within the HSE06 framework (i.e., using a screened version of the PBE0 functional with a screening factor of 0.2 $Å^{-1}$). The only variable parameter is thus the fraction of short-range exact exchange. Figure 2 shows the results of this analysis. The left-hand side shows the variation in the position of the occupied f bands with respect to the E_F as a function of the short-range exact exchange as well as the variations in the direct ($X \rightarrow X$) as well as the indirect ($\Gamma \rightarrow X$) band gap. There are two very interesting features in Fig. 2. The first is the striking linearity in both the band-gap values as well as the f-band position as a function of the short-range exact exchange fraction, with both increasing in absolute value as the percentage of short-range exact exchange increases. The second is the fact that for short-range exact exchange fractions below $\approx 30\%$, all majority band gaps go to zero. The reason for this becomes clear when examining the right-hand side of Fig. 2, which shows two band-structure plots for short-range exact exchange fractions of 44% and 17%, respectively. While in the first case the short-range exact exchange fraction has been fitted to the experimentally observed XPS peak corresponding to the Gd^{3+} $4f^6$ final-state multiplet at $E - E_F = -7.8$ eV, the value of 17% corresponds to an extrapolation to zero gap of the linear fit to the direct majority-spin band gap. For short-range exact exchange fractions of 17% or lower, no majority channel gap is observed as valence and conduction bands merge at the X

point. Lastly, we note that the band structure, calculated using 10% short-range exact exchange, shows the characteristic hole pocket at the Γ point, reported in some early DFT+U work on GdN (see [11] and references therein).

On the basis of the results reported in Fig. 2, it would be possible to use the high degree of linearity, both in the f-level position as well as in the band gap, to fit the fraction of short-range exact exchange to experimental results and thereby obtain a "GdN-optimized" hybrid functional. This attempt is motivated by the demonstrated success of range-separated hybrid functionals in predicting optical gaps, in particular of small-gap semiconductors (Ref. [44] and citations therein). It is important, however, to understand the limitations, or the extent of this success, and so we attempt to fit the contribution of exchange to the band structure to illustrate the complications that may arise. The results of the fits to f-band energies, the direct X-point majority and minority spin gaps, as well as the indirect ($\Gamma \rightarrow X$) band gap are shown in the plot. This being said, fits to current experimental data provide very different results for the short-range exact exchange fraction, depending on which gap value (direct X-point majority and minority and indirect $\Gamma \rightarrow X$) is used. Fitting to the experimental occupied f-level position ($E - E_F = -7.8$ eV [43]) is also problematic since, as pointed out by Leuenberger *et al.* [43], relaxation (screening) effects on the binding energy of the Gd^{3+} $4f^6$ final-state multiplet are likely significant and of unknown magnitude. For all these reasons, we have chosen the standard HSE06 functional for all surface calculations, as its widespread use throughout the literature makes it useful for discussing the qualitative nature of the surface band structure.

B. Surface calculations

A second major issue in the comparison between theoretical calculations and experiment is the degree to which model systems replicate the real material. Defects, in particular N vacancies, are known to be common in the RENs, but equally important for device construction may be the changes in electronic structure induced by the creation of a surface. We build here on the results of the bulk calculations from the previous section to perform calculations of the electronic structure of the GdN(111) surface. The reason for this choice lies in the experimentally observed preference for GdN growth along the [111] direction. The properties of this surface might therefore play a vital role in the interlayer interactions present in GdN-based electronics, such as tunnel junctions, the subject of state-of-the-art research.

We emphasize here that the slab thickness in the model systems was limited by the computational demand caused by high-quality surface calculations. We have therefore investigated more than one structural model of the surface to allow us to cross-check results obtained in each model and identify artifacts of the model construction. These slabs are constructed in either a symmetrical or asymmetrical fashion, whereby we have not considered surface reconstructions, taking only the 1×1 surface unit cell.

The results of the structure relaxations are shown in Fig. 3, where we have indicated the relaxed interlayer distances as well as the unrelaxed interlayer distance equal to 1.44 Å. Notice that relaxation is strong in the top layers of both

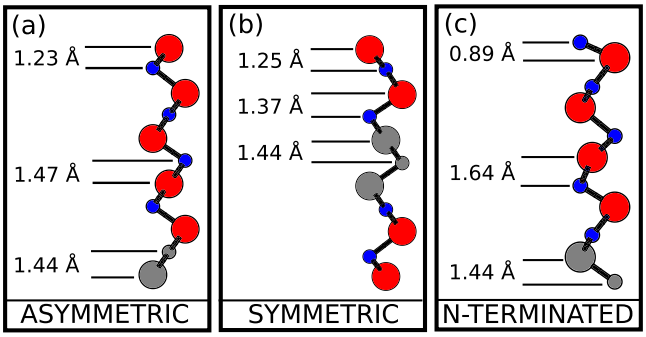

FIG. 3. (Color online) Schematic representation of the structural models used for slab calculations in the case of Gd-terminated (a),(b) and N-terminated slabs (c). The atoms being relaxed are shown in red (Gd) and blue (N), respectively, while atoms being fixed during structure optimization are indicated in gray. Relaxed interlayer distances are indicated for a selected set of relaxed layers. The unrelaxed interlayer distance is also shown for the fixed layers.

Gd-terminated surfaces, but it becomes negligible ($\leqslant 1$)% in the last two relaxed layers of the asymmetric slab. The last relaxed layer in the symmetric slab still shows ≈2.5% of relaxation due to the smaller slab thickness, although, as we will see later, our results on the band structures for both cases show that this does not have a strong influence on the results. In the N-terminated case, on the other hand, there is still strong relaxation ($\geqslant 11$%) in the last relaxed layer. This is due to the low stability of the N-terminated surface, which causes the N atom to be displaced heavily toward the slab, causing the rippling effect in the interlayer distances seen in Fig. 3. Given the apparent instability of the surface, we have not performed any band-structure calculations on the N-terminated surface. All subsequent discussion will therefore focus on the Gd-terminated structures.

Using the relaxed structures, we then performed band-structure calculations along the surface Brillouin zone high-symmetry directions. A band-structure plot of the Gd-terminated GdN(111) surface is shown in Fig. 4. The plot shows the results of both the symmetric as well as the asymmetric slab. Note the similarity between the results of the two calculations. Apart from small differences in band degeneracy, which are due to the extra symmetries present in the symmetric case, both band structures are largely identical. This might be slightly surprising, given the difference in structure as well as the degree to which the last free GdN layer relaxes in the symmetric case. It is in fact precisely due to this remarkable agreement between the band-structure results for the two surface models that we are confident that our surface models are indeed accurate and can be used to discuss the properties of the GdN(111) surface. Although both band-structure plots share all of the important features, there is one notable difference between the two, i.e., the degree to which the conduction band dips below the Fermi energy at the M point. Although the dip persists in the asymmetric case, it is much more pronounced in the symmetric one. Given the difference between the two models, it is likely that the strength of the dip is in part caused by the lower depth to which relaxation is permitted in the symmetric slab. That being said, we stress that the dip does persist in the asymmetric

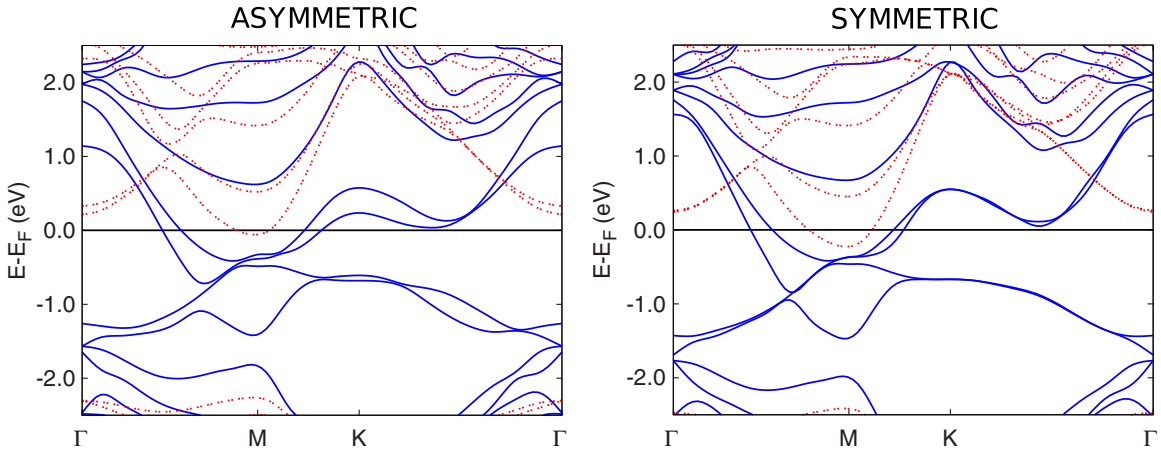

FIG. 4. (Color online) Surface band structure for asymmetric and symmetric Gd-terminated GdN slabs as shown in Fig. 3. Majority and minority spin bands are shown as full-blue and dotted-red lines, respectively.

case, and slab relaxation is only the most probable and not the only explanation for its strength in the symmetric case in comparison to the asymmetric one.

More interesting than the comparison between the two slab models, however, is the comparison of the surface band structure with that of the bulk. While the bulk is a semiconductor with a small direct and a vanishing indirect band gap, the surface clearly shows bands crossing the Fermi energy between the Γ and the M as well as between the M and the K point. On top of this distinctly metallic behavior in the majority-spin channel, the minority-spin channel shows the aforementioned electron pocket at the M point. To verify whether these features are caused by hybridization changes in the surface atoms due to the formation of the slab or are caused instead by a shift in band energies and/or the Fermi energy, we again turn to the local character of the band structure. Care has to be taken here, as all classifications of bands as being due to surface effects must take into account the existence of two surfaces at opposite sides of the slab.

The results of an analysis of the local character of bands in the symmetric slab are shown in Fig. 5. The figure shows the band structure of the GdN(111) surface with projections on the two (top and bottom) surface Gd atoms. As the choice of the percentage of the local contribution that qualifies a band as "surface" is rather arbitrary, we have shown plots for different percentages of the local contribution. Note that, since for local contributions to be evaluated a projection onto spheres surrounding the atoms is performed, the normalization with respect to these spheres of a band at each specific K point is not necessarily constant (or equal to 1). For this reason, the percentages indicated in the figures refer to the percentage that a specific atom (or set of atoms) contributes to the total normalization of the local projection of that band at the K point in question.

Figure 5 provides us with some very valuable information regarding the nature of the changes in band structure that we had observed upon going from bulk GdN to the (111) surface. The first observation that arises from its study is the strong overlap between subfigures (b) and (c) showing pure Gd as well as Gd+N projection for the two surface layers in the symmetric slab, demonstrating the dominant contribution of Gd-localized states for the GdN(111) band structure near E_F. The only two outliers are the point at which the second of the two majority bands crosses the Fermi energy between Γ and M and the lowest-lying majority-spin conduction band at the M point, which show a noticeable N contribution. While surface localization is strong in both the symmetric and the asymmetric case for the bands crossing E_F between M and K, the first band crossing the Fermi energy between Γ and M is rather evenly distributed throughout the slab in the symmetric case. As the corresponding band in the asymmetric slab lines up very well with it, we might use it to gain some further insight.

The corresponding band structure and projection are shown in Fig. 5(d). Interestingly, it shows that the band, poorly localized in the symmetric case, displays heavy localization on the unrelaxed surface layer for the asymmetric case. The fact that this does not lead to a significant change in the band structure likely indicates that the band is indeed a surface band, but the slow decay toward the bulk makes it impossible to identify it as such in the symmetric slab. This difference between the asymmetric and symmetric slabs highlights the importance of our dual model for the surface. The unrelaxed surface in the asymmetric slab is merely a computational artifact, which might suggest that the symmetric slab is a better model for the description of the surface states. However, the asymmetric slab allows for a more extensive relaxation of the surface and a larger bulklike region. The correspondence between the two models is therefore important for the robustness of the conclusions that we are able to draw.

This still leaves the minority-spin electron pocket centered around the M point unaccounted for. To investigate its origin, in Fig. 6 we have plotted the local character of the bands as projected onto the central Gd atoms of the slab only. The results show very clearly that the M-point electron pocket, in contrast to the majority channel metallic states, is dominated by states lying at the center of the slab.

To provide further evidence for this explanation, Fig. 6 also shows a partial charge density, as integrated over the band forming the electron pocket at the M point. This image reinforces our conclusion that the electron pocket is due to GdN-bulk states in the slab. It further clearly shows that there is only a negligible contribution from the N atoms. The origin

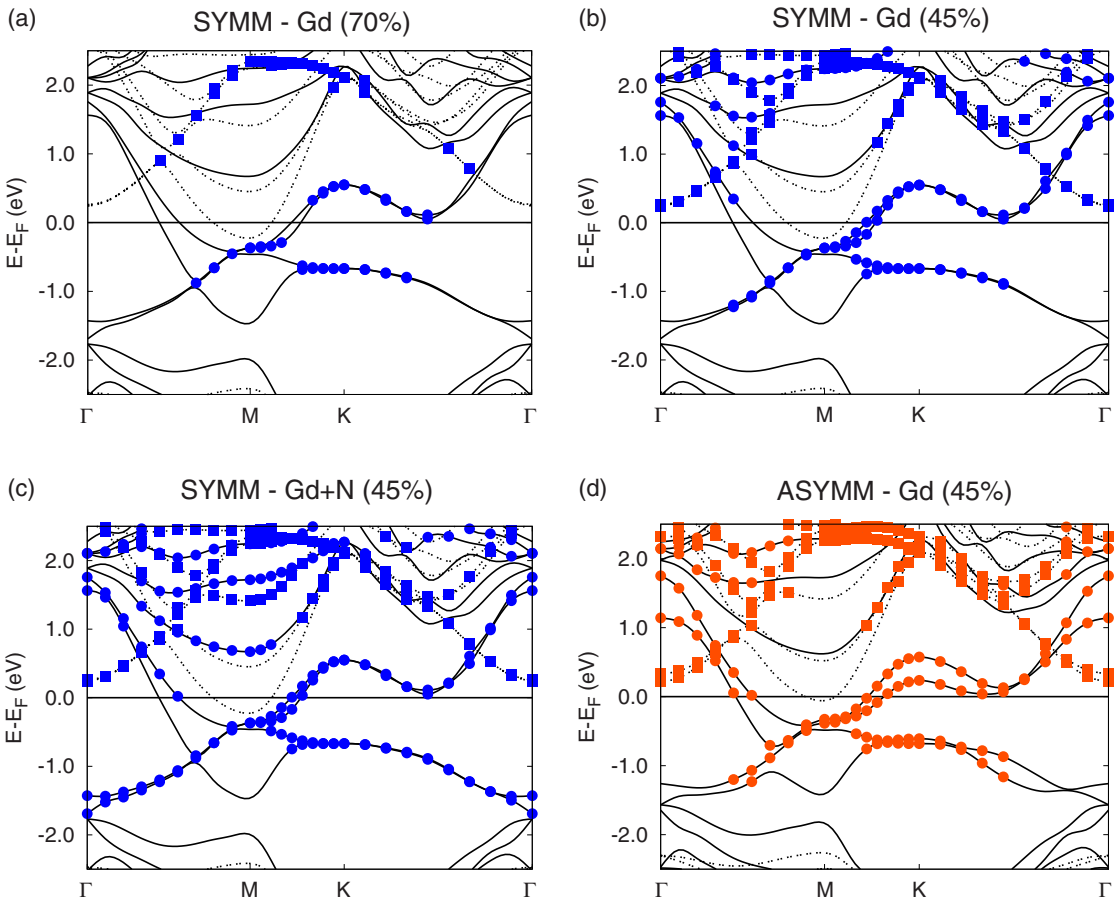

FIG. 5. (Color online) Surface band structure for a symmetric/asymmetric, Gd-terminated slab as shown in Fig. 3. The figure also shows the local contribution by two (top and bottom) surface layers as defined by the first Gd/Gd+N atomic layers as indicated above the plots. Subplots (a) and (b) show different degrees of Gd contribution for the symmetric slab, while (c) shows a summed (Gd+N) contribution for the same case. Subplot (d), on the other hand, shows the Gd contribution for the asymmetric case. Blue circles (squares) indicate majority (minority) -spin bands where the sum of local contributions is greater than or equal to the percentage indicated in the parentheses. Red symbols, on the other hand, correspond to an analogous projection for the asymmetric, Gd-terminated slab. In all cases, majority- and minority-spin bands are again shown as full and dotted lines, respectively.

of this feature likely lies in the bulk conduction bands being pushed below E_F for the surface, either by a change in the band energy or by a repositioning of E_F due to the formation of the slab. The change in depth of the electron pocket between the symmetric and asymmetric slabs suggests that this feature is indeed sensitive to slab thickness.

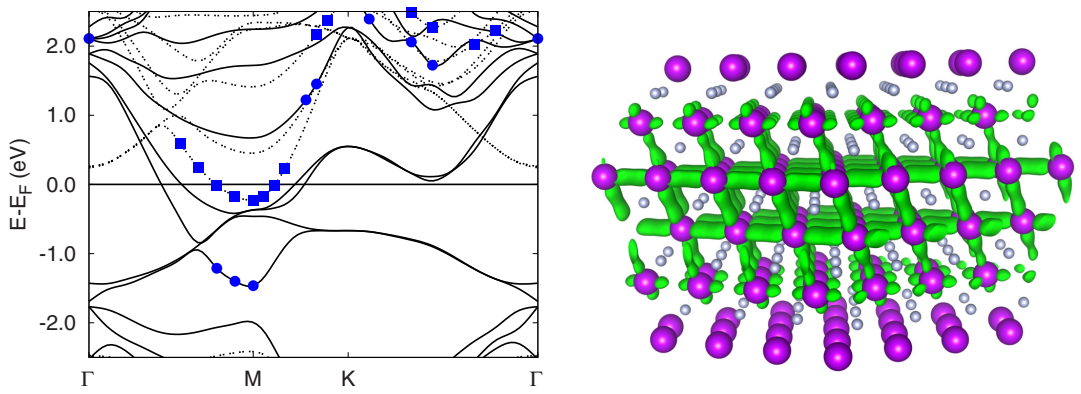

FIG. 6. (Color online) Surface band structure for a symmetric, Gd-terminated GdN slab as shown in Fig. 3. Blue symbols indicate bands with summed local contributions by the two central Gd atoms $\geqslant$40%. On the right-hand side, a 3D plot of the partial charge density corresponding to the band forming the electron pocket at the M point is also shown. Note that the partial charge density is *not* integrated over all of k space and corresponds *only* to the M point itself. Green isosurfaces have been drawn at $1.0 \times 10^{-4}\ e/a_0^3$.

IV. CONCLUSION

The present work has demonstrated the ability of state-of-the-art plane-wave hybrid-DFT methods to provide valuable insights into the behavior of difficult-to-model rare-earth nitride systems. We have considered in detail the effect of the fraction of short-range exact exchange on the band gap and the f-band energy in bulk GdN, and we showed how they might be exploited in the future to create custom-tailored hybrid functionals for the study of rare-earth nitrides. We have further shown how high-level theoretical models might be applied to surface calculations for the case of GdN(111) surfaces, where we have performed band-structure calculations on a rare-earth nitride surface using the HSE06 screened hybrid functional. The insights gained from our calculations should be valuable to experimentalists, and provide a motivation for further theoretical research into this fascinating area of materials science.

ACKNOWLEDGMENTS

The authors would like to thank F. Natali, H. J. Trodahl, and M. Quennet for interesting discussions and helpful comments. The High Performance Computing Network of Northern Germany (HLRN), Science Faculty HPC Facility at Victoria University of Wellington, and the computer facilities at Freie Universität Berlin (ZEDAT) are acknowledged for computer time. L.E.M.S. further acknowledges the financial support by the International Max Planck Research School "Complex Surfaces in Material Sciences" as well as Victoria University of Wellington. The XCRYSDEN [45] and VESTA [46] programs were used to create images of atomic structures throughout this work.

[1] G. Binasch, P. Grünberg, F. Saurenbach, and W. Zinn, Phys. Rev. B **39**, 4828 (1989).
[2] P. A. Grünberg, Rev. Mod. Phys. **80**, 1531 (2008).
[3] J. Barnaś, A. Fuss, R. E. Camley, P. Grünberg, and W. Zinn, Phys. Rev. B **42**, 8110 (1990).
[4] S. Wolf, D. Awschalom, R. Buhrman, J. Daughton, S. Von Molnar, M. Roukes, A. Y. Chtchelkanova, and D. Treger, Science **294**, 1488 (2001).
[5] F. Natali, B. J. Ruck, N. O. Plank, H. J. Trodahl, S. Granville, C. Meyer, and W. R. Lambrecht, Prog. Mater. Sci. **58**, 1316 (2013).
[6] A. I. Liechtenstein, V. I. Anisimov, and J. Zaanen, Phys. Rev. B **52**, R5467(R) (1995).
[7] P. Larson and W. R. L. Lambrecht, Phys. Rev. B **74**, 085108 (2006).
[8] M. Geshi, K. Kusakabe, and N. Suzuki, J. Phys. Condens. Matter **16**, S5701 (2004).
[9] A. Punya, T. Cheiwchanchamnangij, A. Thiess, and W. R. L. Lambrecht, MRS Proceedings **1290**, mrsf10-1290 (2011).
[10] C. Mitra and W. R. L. Lambrecht, Phys. Rev. B **78**, 134421 (2008).
[11] C.-G. Duan, R. Sabirianov, W. Mei, P. A. Dowben, S. Jaswal, and E. Y. Tsymbal, J. Phys. Condens. Matter **19**, 315220 (2007).
[12] G. M. Dalpian and S.-H. Wei, Phys. Rev. B **72**, 115201 (2005).
[13] C. Mitra and W. R. L. Lambrecht, Phys. Rev. B **78**, 195203 (2008).
[14] H. J. Trodahl, A. R. H. Preston, J. Zhong, B. J. Ruck, N. M. Strickland, C. Mitra, and W. R. L. Lambrecht, Phys. Rev. B **76**, 085211 (2007).
[15] P. Larson, W. R. L. Lambrecht, A. Chantis, and M. van Schilfgaarde, Phys. Rev. B **75**, 045114 (2007).
[16] C.-G. Duan, R. F. Sabiryanov, J. Liu, W. N. Mei, P. A. Dowben, and J. R. Hardy, Phys. Rev. Lett. **94**, 237201 (2005).
[17] V. N. Antonov, B. N. Harmon, A. N. Yaresko, and A. P. Shpak, Phys. Rev. B **75**, 184422 (2007).
[18] S. Abdelouahed and M. Alouani, Phys. Rev. B **76**, 214409 (2007).
[19] I. N. Sivkov, O. O. Brovko, and V. S. Stepanyuk, Phys. Rev. B **89**, 195419 (2014).
[20] T. Kagawa and H. Raebiger, Phys. Rev. Appl. **2**, 054009 (2014).
[21] S. Abdelouahed, and M. Alouani, Phys. Rev. B **79**, 054406 (2009).
[22] M. Schlipf, M. Betzinger, C. Friedrich, M. Ležaić, and S. Blügel, Phys. Rev. B **84**, 125142 (2011).
[23] M. Schlipf, M. Betzinger, C. Friedrich, M. Ležaić, and S. Blügel, Phys. Rev. B **90**, 239908(E) (2014).
[24] A. N. Chantis, M. van Schilfgaarde, and T. Kotani, Phys. Rev. B **76**, 165126 (2007).
[25] K. Doll, J. Phys. Condens. Matter **20**, 075214 (2008).
[26] C. M. Aerts, P. Strange, M. Horne, W. M. Temmerman, Z. Szotek, and A. Svane, Phys. Rev. B **69**, 045115 (2004).
[27] W. R. L. Lambrecht, Phys. Rev. B **62**, 13538 (2000).
[28] S. Kalvoda, M. Dolg, H.-J. Flad, P. Fulde, and H. Stoll, Phys. Rev. B **57**, 2127 (1998).
[29] G. Kresse and J. Hafner, Phys. Rev. B **47**, 558 (1993).
[30] G. Kresse and J. Hafner, Phys. Rev. B **49**, 14251 (1994).
[31] G. Kresse and J. Furthmüller, Comput. Mater. Sci. **6**, 15 (1996).
[32] G. Kresse and J. Furthmüller, Phys. Rev. B **54**, 11169 (1996).
[33] P. E. Blöchl, Phys. Rev. B **50**, 17953 (1994).
[34] G. Kresse and D. Joubert, Phys. Rev. B **59**, 1758 (1999).
[35] A. V. Krukau, O. A. Vydrov, A. F. Izmaylov, and G. E. Scuseria, J. Chem. Phys. **125**, 224106 (2006).
[36] T. M. Henderson, J. Paier, and G. E. Scuseria, Phys. Status Solidi B **248**, 767 (2011).
[37] J. Paier, M. Marsman, K. Hummer, G. Kresse, I. Gerber, and J. Ángyán, J. Chem. Phys. **125**, 9901 (2006).
[38] J. Paier, M. Marsman, K. Hummer, G. Kresse, I. C. Gerber, and J. G. Ángyán, The J. Chem. Phys. **124**, 154709 (2006).
[39] J. Heyd, G. E. Scuseria, and M. Ernzerhof, The J. Chem. Phys. **118**, 8207 (2003).
[40] D. Li, Y. Haga, H. Shida, T. Suzuki, Y. Kwon, and G. Kido, J. Phys. Condens. Matter **9**, 10777 (1997).
[41] R. Vidyasagar, T. Kita, T. Sakurai, and H. Ohta, J. Appl. Phys. **115**, 203717 (2014).
[42] A. G. Petukhov, W. R. L. Lambrecht, and B. Segall, Phys. Rev. B **53**, 4324 (1996).
[43] F. Leuenberger, A. Parge, W. Felsch, K. Fauth, and M. Hessler, Phys. Rev. B **72**, 014427 (2005).
[44] B. G. Janesko, T. M. Henderson, and G. E. Scuseria, Phys. Chem. Chem. Phys. **11**, 443 (2009).
[45] A. Kokalj, Proceedings of the Symposium on Software Development for Process and Materials Design [Comput. Mater. Sci. **28**, 155 (2003)] .
[46] K. Momma and F. Izumi, J. Appl. Crystallogr., **44**, 1272 (2011).